

Twisted Intramolecular Charge Transfer State for Long-Wavelength Thermally Activated Delayed Fluorescence

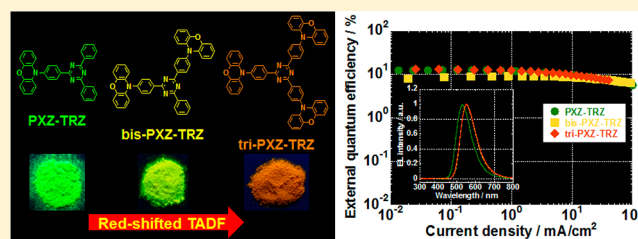
Hiroyuki Tanaka,[†] Katsuyuki Shizu,[†] Hajime Nakanotani,^{†,‡} and Chihaya Adachi^{*,†,‡,§}[†]Center for Organic Photonics and Electronics Research (OPERA), Kyushu University, 744 Motooka, Nishi, Fukuoka 819-0395, Japan[‡]Innovative Organic Device Laboratory, Institute of Systems, Information Technologies and Nano-Technologies (ISIT), 744 Motooka, Nishi, Fukuoka 819-0395, Japan[§]International Institute for Carbon Neutral Energy Research (WPI-I2CNER), Kyushu University, 744 Motooka, Nishi, Fukuoka 819-0395, Japan

Supporting Information

ABSTRACT: Emission wavelength tuning of thermally activated delayed fluorescence from green to orange in solid state films is demonstrated. Emission tuning occurs by stabilization of the intramolecular charge transfer state between a phenoxazine (PXZ) donor unit and 2,4,6-triphenyl-1,3,5-triazine (TRZ) acceptor unit separated by a large twist angle. The emission wavelengths of mono-, bis-, and tri-PXZ-substituted TRZ exhibit a gradual red shift while maintaining a small energy gap between the singlet and triplet excited states.

An organic light-emitting diode containing a tri-PXZ-TRZ emitter exhibited a maximum external quantum efficiency of $13.3 \pm 0.5\%$ with yellow-orange emission.

KEYWORDS: organic light-emitting diodes, thermally activated delayed fluorescence, emission wavelength tuning, intramolecular charge transfer



INTRODUCTION

Since our group reported the first observation of electroluminescence (EL) based on thermally activated delayed fluorescence (TADF) from a Sn^{4+} -porphyrin complex,¹ the potential of TADF materials as emitters for organic light-emitting diodes (OLEDs) has been revealed.² A remarkable feature of TADF is up-conversion of excitons from the lowest triplet excited state (T_1) of a compound to its lowest singlet excited state (S_1), which strongly depends on the energy gap between them ($\Delta E_{S,T}$). Up-conversion from T_1 to S_1 can be realized in molecules with donor-acceptor (D-A) moieties that induce intramolecular charge transfer (ICT). TADF materials are currently attracting considerable attention as third-generation OLEDs because of their high EL efficiency and lack of rare metals such as Ir and Pt. To replace the present OLEDs based on fluorescent and phosphorescent materials, methodology for RGB emission wavelength tuning is essential. The emission process of general fluorescent materials involves $\pi-\pi^*$ transitions via singlet excitons, and emission wavelength tuning is achieved by controlling the length of π -conjugation. Attaching substituents such as electron-donating or -withdrawing groups to fluorescent molecules is also an effective way to tune emission wavelength.³ Conversely, the emission process of typical phosphorescent materials such as iridium complexes is based on triplet metal-to-ligand charge transfer ($^3\text{MLCT}$)

transitions. Their emission wavelength has also been tuned by extending the conjugation of the ligand.⁴

In the case of TADF materials, the emission process is categorized as ICT transitions via triplet excitons. To minimize $\Delta E_{S,T}$ for efficient up-conversion, a TADF molecule needs its highest occupied molecular orbital (HOMO) and lowest unoccupied molecular orbital (LUMO) to be effectively separated, which can be achieved using a twisted structure. Effective HOMO-LUMO separation induces the ICT transition from HOMO to LUMO. Regarding the molecular design of TADF materials, simple extension of the π -conjugated system results in a large $\Delta E_{S,T}$ and weak ICT transition, which induces a locally excited state and dual fluorescence.⁵ While efficient blue^{2,6} and green^{2,7} TADF materials have been fabricated using various molecular designs that suitably connect the donor and acceptor units, there are currently few examples of orange-red TADF materials.^{1,2} The limitation of molecular design means that, efficient red TADF is undeveloped compared with blue and green TADF.

Because TADF is a charge transfer (CT) emission from ICT-type luminescent materials with small $\Delta E_{S,T}$, control of the ICT state must affect the emission wavelength of TADF. We

Received: July 18, 2013

Revised: September 1, 2013

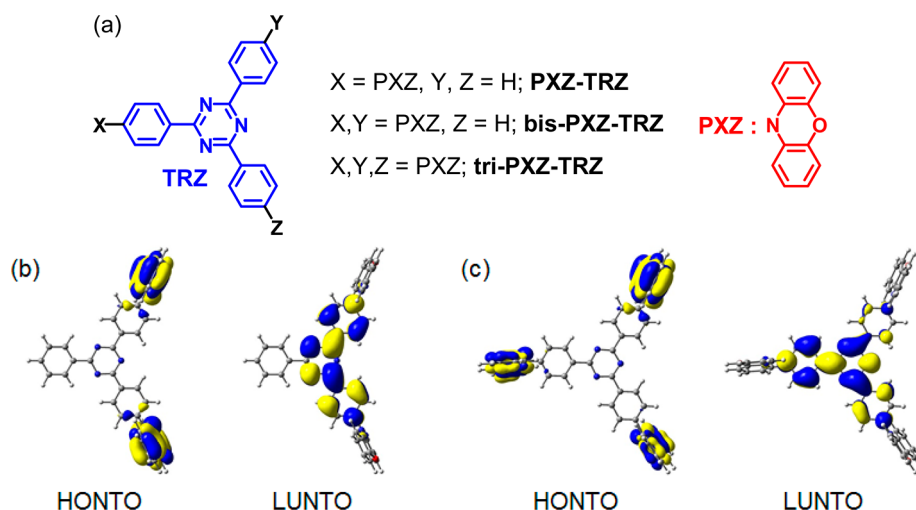


Figure 1. (a) Molecular structures of branched PXZ-TRZ type TADF molecules. One branch, PXZ-TRZ; two branches, bis-PXZ-TRZ; three branches, tri-PXZ-TRZ. (b,c) Highest occupied and lowest unoccupied natural transition orbitals (HONTO and LUNTO, respectively) of bis-PXZ-TRZ and tri-PXZ-TRZ, respectively, calculated at TD- ω B97X-D/cc-pVDZ level.

recently reported a green TADF emitter, PXZ-TRZ, with a small $\Delta E_{S,T}$.^{7b} PXZ-TRZ has a typical twisted ICT (TICT) state,⁸ with phenoxazine (PXZ) as a donor unit and triphenyl-triazine (TRZ) as an acceptor unit. As a model molecular system to control the ICT state of TADF materials, we designed a branched TICT-type D–A system, in which PXZ was attached to the *para*-position of the terminal phenyl rings of the TRZ acceptor core unit, as shown in Figure 1. In this article, we demonstrate that the emission wavelength of TADF can be tuned in the long-wavelength region using the branched PXZ-TRZ-type TADF materials bis-PXZ-TRZ (D_2 -A) and tri-PXZ-TRZ (D_3 -A).

RESULTS AND DISCUSSION

To estimate the frontier molecular orbitals of the designed molecules, we performed density functional theory (DFT) calculations. First, the ground-state geometries were optimized with Gaussian 09 software⁹ using the ω B97X-D functional¹⁰ and cc-pVDZ basis set.¹¹ The geometrical parameters of the optimized ground state of bis-PXZ-TRZ agreed well with those derived from its X-ray structure. The molecular structures and highest occupied and lowest unoccupied natural transition orbitals (HONTO and LUNTO, respectively)¹² for the optimized ground-state geometries of the molecules are shown in Figure 1. The optimized geometries of bis-PXZ-TRZ and tri-PXZ-TRZ have a large twist angle between the donor and acceptor planes, similar to PXZ-TRZ. The dihedral angles between PXZ and TRZ units were calculated to be about 82° for bis-PXZ-TRZ and 81° for tri-PXZ-TRZ. Dihedral angles estimated from X-ray structure analysis of the compounds were about 88° , which agreed with the calculated values. An ORTEP (Oak Ridge Thermal-Ellipsoid Plot Program) drawing showing the twisted structure of bis-PXZ-TRZ is depicted in Figure 2 (see Supporting Information for details). The phenyl rings of the TRZ acceptor core unit were almost coplanar. The twist between PXZ and TRZ units suppressed the delocalization of electron density distribution of the HONTO and LUNTO. The HONTOs are mainly distributed on the PXZ moieties, while the LUNTO is localized on the TRZ moiety. The molecular structure of bis-PXZ-TRZ determined by X-ray analysis almost corresponded to the

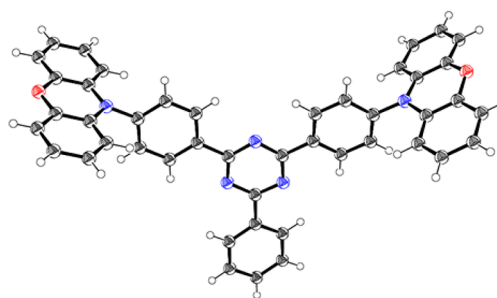


Figure 2. ORTEP drawing of bis-PXZ-TRZ. Thermal ellipsoids are drawn at the 50% probability level. A solvent molecule (toluene) is omitted for clarity.

optimized structure estimated from the DFT calculation. There was a small overlap of HONTO and LUNTO at the phenyl ring connecting PXZ and TRZ. To investigate the low-lying excited states of the molecules, we calculated the 10 lowest singlet and triplet excited states for their optimized ground-state geometries by time-dependent DFT^{13,14} (TD-DFT) calculations using the same functional and basis set (denoted as TD- ω B97X-D/cc-pVDZ). As expected from the electron density distribution of the frontier molecular orbitals and the results of X-ray crystal structure analysis, the estimated $\Delta E_{S,T}$ values were quite small (those of bis-PXZ-TRZ and tri-PXZ-TRZ were 0.054 and 0.065 eV, respectively). These results indicate that the twist between PXZ and TRZ moieties induced effective separation of HONTO and LUNTO and TICT excited states, similar to PXZ-TRZ with a small $\Delta E_{S,T}$ of 0.070 eV (see Supporting Information for details).

To investigate the effect of attaching different numbers of PXZ donor units to a TRZ acceptor core unit on emission wavelength, we measured UV–vis absorption and photoluminescence (PL) spectra of the compounds in toluene solution (Figure 3). The absorption spectra of the three molecules exhibited CT absorption between 365 and 500 nm derived from electron transfer from the HOMO to LUMO. The intensity of the CT absorption gradually increased and the maximum also red-shifted as the number of PXZ donor units increased. We estimated the HOMO–LUMO gaps of the three compounds from the onset positions of their absorption spectra

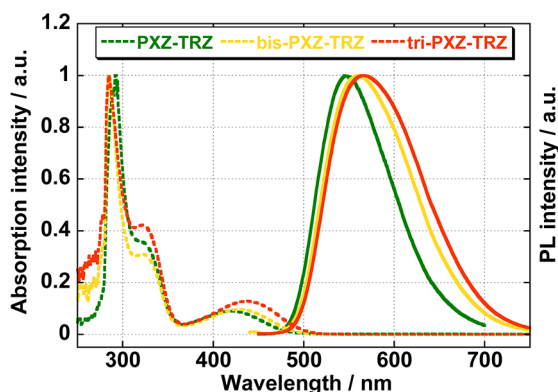


Figure 3. Normalized absorption (dashed lines) and PL (solid lines) spectra of PXZ-TRZ (green), bis-PXZ-TRZ (yellow), and tri-PXZ-TRZ (orange) in toluene solution with a concentration of 1.0×10^{-5} M.

(see Supporting Information for details). The HOMO–LUMO gaps gradually decreased as the number of PXZ donor units increased. These results indicate that the ICT state is stabilized by an increased number of PXZ donor units. The emission maxima and color for mono-, bis-, and tri-PXZ-TRZ were 545 nm (green), 560 nm (yellow), and 568 nm (yellow-orange), respectively. In particular, the half-width of the emission spectrum increased considerably with the attachment of PXZ donor units. Although the onset of the emission spectra of these three compounds was almost the same, the half-width of emission increased from 94 nm for PXZ-TRZ to 120 nm for tri-PXZ-TRZ. This broadening indicates that ICT is enhanced as the number of PX donor units increases, which was observed as an increase of the intensity of the CT absorption.

Generally, the photophysical properties of molecular systems with an ICT state exhibit solvatochromism, in which the emission wavelength undergoes a large red shift as the polarity of the solvent increases.¹⁵ To verify the stability of the ICT states of the three compounds, we studied their photophysical properties in various solvents. The emission maxima exhibited a gradual red shift as the polarity of the solvent increased. The emission maxima (ν_{\max} in wavenumber) are plotted against the solvent polarity parameter $E_T(30)$ in Figure 4.¹⁵ The compounds exhibited positive solvatochromism, with emission maxima depending approximately linearly on solvent polarity.

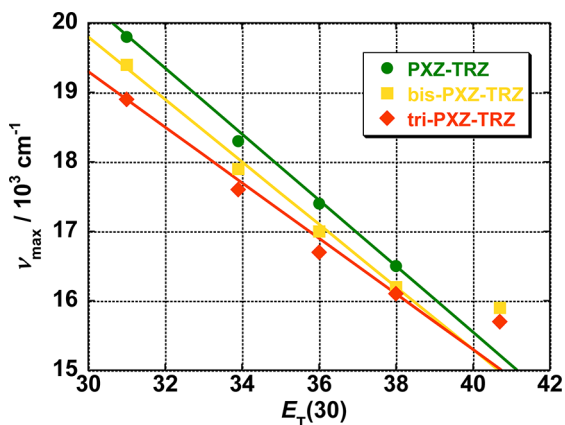


Figure 4. Dependence of the emission maxima for PXZ-TRZ (green), bis-PXZ-TRZ (yellow), and tri-PXZ-TRZ (orange) on the solvent polarity parameter $E_T(30)$.

The dependence on solvent polarity decreased as the number of PXZ donor units increased. This result indicates that the ICT state of tri-PXZ-TRZ is the most stable among the three compounds and enhancement of the donor property of PXZ-TRZ stabilizes the ICT state. In addition, the stabilization of the ICT state induces the broadening of the CT emission (see Supporting Information).

The small $\Delta E_{S,T}$ values of the three compounds allow efficient up-conversion of excitons from the T_1 to the S_1 state through reverse intersystem crossing (RISC) and increase their emission quantum yield. The up-conversion phenomenon can be observed as a delayed fluorescence component with a lifetime of micro- to millisecond order after a nanosecond-order prompt fluorescence component. To study the effect of an increased number of PXZ donor units on PL lifetime, we observed the transient PL decay profiles of the three compounds in toluene solution. It is known that the triplet excitons of TADF materials are inactivated by included triplet oxygen molecules (3O_2). Therefore, lifetime profiles were measured after deoxygenation of the solutions by bubbling nitrogen through them. The PL quantum yields (ϕ_{PL}) of the three compounds increased from ca. 12–14% (prompt component only) to ca. 23–29% (prompt and delayed components) upon deoxygenation. The transient PL decay profiles of the three compounds are depicted in Figure 5. The

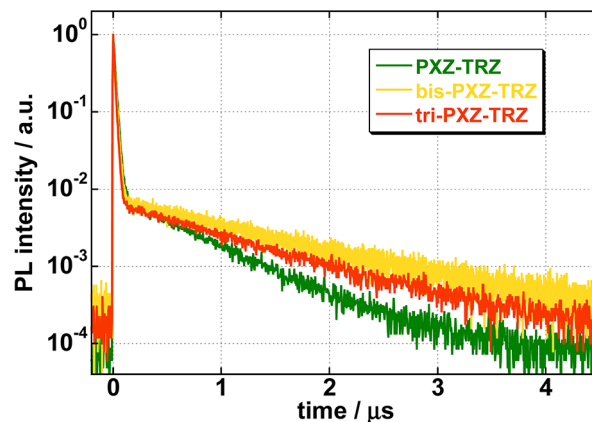


Figure 5. Transient PL decay profiles of PXZ-TRZ (green), bis-PXZ-TRZ (yellow), and tri-PXZ-TRZ (orange) in toluene solution at a concentration of 1.0×10^{-5} M.

transient decay profiles obviously had two components. The first was assigned to the prompt component derived from the direct $S_1 \rightarrow S_0$ transition, which has a lifetime (τ_1) of ca. 17 ns. The second can be assigned to the delayed component resulting from the recursive $S_1 \rightarrow S_0$ transition via successive RISC and up-conversion of the excitons from the T_1 state, which exhibited a lifetime (τ_2) that lengthened from 0.68 μ s for PXZ-TRZ to over 1 μ s for bis- and tri-PXZ-TRZ. This behavior can be explained by considering the half-width of CT emission from the compounds in toluene solutions. The half-width of PXZ-TRZ emission was the narrowest among the three compounds. The narrow width of the CT emission indicates the ICT excited state was localized on the single D–A structure, which results in the shortest lifetime (τ_2 is 0.68 μ s) among the three compounds. The half-widths of bis- and tri-PXZ-TRZ were wider than that of PXZ-TRZ (Figure 3), indicating that the ICT excited state was delocalized over the PXZ donor units and TRZ acceptor core unit in these

compounds. Such delocalization of the ICT state over the multiple D–A structures stabilizes it.¹⁶ The energy of the delocalized ICT excited state is changed by the torsional disorder between the PXZ donor units and the TRZ acceptor unit, which lengthen the lifetime (τ_2 were 1.33 and 1.10 μ s for bis- and tri-PXZ-TRZ, respectively). However, τ_2 of tri-PXZ-TRZ was shorter than that of bis-PXZ-TRZ. This is attributed to increased vibrational nonradiative deactivation of the excitons of tri-PXZ-TRZ via solvent molecules compared to those of bis-PXZ-TRZ. To verify the thermal activation of the observed transient PL decay profiles, we investigated the temperature dependence of the PL spectrum of 6 wt % doped films of bis- and tri-PXZ-TRZ in 3,3'-bis(*N*-carbazolyl)-1,1'-biphenyl (mCBP) as a host using a streak camera (Figures S4–S9, Supporting Information). As the temperature was increased from 10 K, the ϕ_{PL} of the delayed components of bis- and tri-PXZ-TRZ gradually increased and reached 50% and 40% at 300 K, respectively. These results confirm that bis- and tri-PXZ-TRZ are TADF materials.

We fabricated OLEDs containing bis- or tri-PXZ-TRZ as TADF emitters with structures of indium tin oxide (ITO)/*N,N'*-diphenyl-*N,N'*-bis(1-naphthyl)-1,10-biphenyl-4,4'-diamine (α -NPD) (35 nm)/6 wt % bis- or tri-PXZ-TRZ:mCBP (15 nm)/1,3,5-tris(2-*N*-phenylbenzimidazolyl) benzene (TPBi) (65 nm)/LiF (0.8 nm)/Al (80 nm). The HOMO and LUMO levels of bis- and tri-PXZ-TRZ were estimated to be 5.7 and 3.4 eV, respectively, from the UV–vis absorption spectra of neat films and work function measurements. To confine generated excitons in the emitting layer, mCBP was selected as the host material because it has a wider HOMO–LUMO gap than bis- and tri-PXZ-TRZ (Figures S10 and S11, Supporting Information). The OLED characteristics of bis- and tri-PXZ-TRZ are shown as yellow and orange plots in Figure 6,

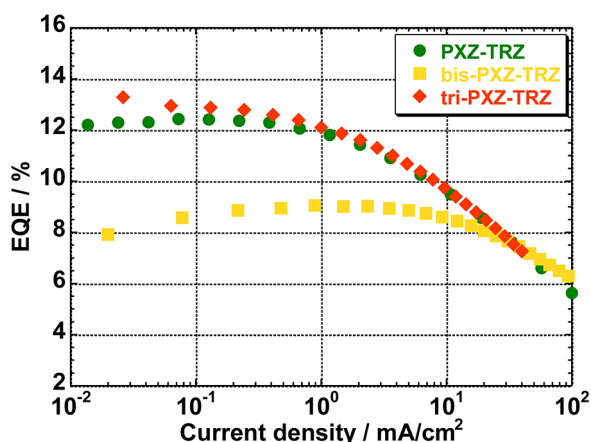


Figure 6. Dependence of EQE on current density for PXZ-TRZ (green), bis-PXZ-TRZ (yellow), and tri-PXZ-TRZ (orange).

respectively. For the OLED containing tri-PXZ-TRZ, the external quantum efficiency (EQE) vs. current density plots exhibited a maximum EQE of $13.3 \pm 0.5\%$, and the dependence of EQE on the current density behaved similar to that of PXZ-TRZ as shown by green and orange plots. In contrast to mono- and tri-PXZ-TRZ, the EQE vs. current density plots of bis-PXZ-TRZ exhibited a maximum EQE of $9.1 \pm 0.5\%$, and the value was lower than those of mono- and tri-PXZ-TRZ. On the basis of the results of the temperature-dependence of the transient PL spectra of bis- and tri-PXZ-TRZ, we estimated the

OLED characteristics (see Supporting Information for details). Although the ϕ_{PL} of 6 wt % bis- and tri-PXZ-TRZ doped films in mCBP were 64 and 58%, respectively, the EQE values showed a large difference of near 4%. From the estimations, the reason can be attributed to a difference of $\gamma\eta_{\text{out}}$, where γ is the ratio of the charge injection to the electron and hole transportation and η_{out} is the out-coupling constant. The $\gamma\eta_{\text{out}}$ values of bis- and tri-PXZ-TRZ were 0.153 and 0.260, respectively. These estimated values indicate a morphological difference of the 6 wt % bis- and tri-PXZ-TRZ doped films in mCBP. However, these results substantially exceed the theoretical limit of general fluorescent materials (5–7% assuming an outcoupling efficiency of 0.2–0.3). These high EQEs are attributed to the efficient up-conversion of triplet excitons to the S_1 state, as for PXZ-TRZ.^{7b} Figure 7 shows the

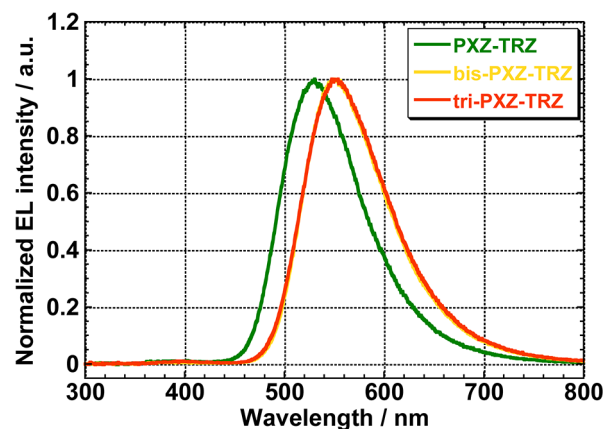


Figure 7. Normalized EL spectra from the OLEDs containing PXZ-TRZ (green), bis-PXZ-TRZ (yellow), or tri-PXZ-TRZ (orange).

EL spectra from the OLEDs containing mono-, bis-, or tri-PXZ-TRZ. The EL spectra of bis- and tri-PXZ-TRZ almost overlapped and yellow-orange EL spectra were observed at around 552 nm. For the EL spectra, the half-width slightly increased from 92 (PXZ-TRZ) to 98 nm (tri-PXZ-TRZ) and the maximum red-shifted from 529 (PXZ-TRZ) to 553 nm (tri-PXZ-TRZ) as the number of PXZ donor units increased.

CONCLUSIONS

We tuned the emission wavelength of TADF materials from green to orange using branched PXZ-TRZ-type molecules with small $\Delta E_{\text{S,T}}$. Importantly, the branched PXZ-TRZ molecules maintained high EQE of around 9–13%. Enhancement of the donor property by increasing the number of PXZ donor units induces the delocalization of the ICT state over the multiple D–A structures. This stabilizes the ICT state, causing the CT emission to exhibit a red shift and broaden. These results offer a powerful methodology to realize efficient red TADF emitters, which differs from the tuning strategy of fluorescent and phosphorescent materials of extending the conjugated system. Effective modification of the frontier orbitals to achieve red TADF is in progress.

EXPERIMENTAL SECTION

General Procedures. Starting materials were purchased from Wako Pure Chemical Industries, Ltd., Tokyo Chemical Industry Co., Ltd., and Sigma-Aldrich Co. and used without further purification, unless otherwise stated. UV–vis spectra were recorded on a Shimadzu UV–vis absorption spectrometer UV2550 for the solution states and

the solid states. Fluorescence spectra were recorded on a Horiba Jovan Yvon FluoroMax-4 spectrometer for the solution states and the solid states. PL quantum yield (ϕ_{PL}) in the solution states were measured with a Hamamatsu absolute PL quantum yield spectrometer C11347 (Quantaury-QY). Transient PL decay profiles in the solution states at ambient temperature were measured with Hamamatsu compact fluorescence lifetime spectrometer C11367 (Quantaury-Tau). The temperature dependence of the transient PL decay profiles was measured with a Hamamatsu streak camera system C4334 equipped with an IWATANI cryostat GASESCRT-006-2000. A Lasertechnik Berlin nitrogen gas laser MNL200 with an excitation wavelength of 337 nm was used. The codeposited films were fabricated by a thermal deposition. The OLED characteristics were evaluated at ambient temperature using an Agilent semiconductor parameter analyzer E5273A. NMR spectra used in the characterization of products were recorded on a JEOL-ECP400 400 MHz spectrometer. All NMR spectra were referenced to solvent. Matrix-assisted laser desorption/ionization time-of-flight mass spectrometry (MALDI-TOF-MS) were recorded on a Bruker Daltonics Autoflex III spectrometer using positive mode.

2,4-Bis(4-bromophenyl)-6-phenyl-1,3,5-triazine. A mixture of 1.55 g of benzoyl chloride (11.0 mmol) and 4.00 g of 4-bromobenzonitrile (22.0 mmol) in 15 mL of dichloromethane was cooled at 0–5 °C by ice-bath and stirred for 30 min. Then, 3.30 g of antimony chloride (11.0 mmol) was added dropwise to the above solution. The mixture was stirred at room temperature for one hour and further stirred and refluxed overnight. The cooled mixture was filtrated, and the collected yellow solid was washed by dichloromethane. The solid was slowly added to 75 mL of 28% ammonia solution cooled at 0–5 °C by ice-bath and stirred for 30 min at same temperature. Then the mixture was stirred for 3 h at room temperature. Subsequently, the mixture was filtrated, and the collected white solid was washed by water. The solid was added to 30 mL of *N,N'*-dimethylformamide and stirred at 155 °C for 30 min. The insoluble solid was separated by the filtration. The filtration was repeated 3 times. Then the solvent was removed under vacuum, and 2.55 g of 2,4-bis(4-bromophenyl)-6-phenyl-1,3,5-triazine was obtained as a white solid. The yield was over 50%. This material was used at next step without a further purification. [NMR] ^1H NMR (CDCl_3 , 300 MHz) δ = 7.47 (m, 3H), 7.70 (d, 4H), 8.62 (d, 4H), 8.73 (d, 2H); ^{13}C NMR (CDCl_3 , 300 MHz) δ = 113.3, 115.7, 121.9, 123.3, 127.0, 129.2, 129.7, 131.8, 131.9, 133.7, 142.4, 144.0. [MS] MALDI-TOF-MS m/z calcd for $\text{C}_{21}\text{H}_{13}\text{Br}_2\text{N}_3$, 467; found, 467.

2,4-Bis(4-(10*H*-phenoxazin-10*H*-yl)phenyl)-6-phenyl-1,3,5-triazine (bis-PXZ-TRZ). To a solution of 1.40 g of 2,4-bis(4-bromophenyl)-6-phenyl-1,3,5-triazine (3.00 mmol), 1.21 g of phenoxazine (6.60 mmol), and 2.74 g of potassium carbonate (19.8 mmol) in 50 mL of toluene was added, with stirring, a solution of 44.9 mg of palladium (II) acetate (0.20 mmol) and 148 mg of tri-*tert*-butylphosphine (0.73 mmol) in 50 mL of toluene. Subsequently, the mixture was stirred and refluxed for one day. The cooled mixture was partitioned between chloroform and water. The organic layer was separated, and the aqueous layer was extracted with chloroform. The combined organic layers were washed with brine, dried over Mg_2SO_4 , and concentrated in vacuo. Column chromatography of the residue solid (eluent, chloroform) afforded 1.69 g of bis-PXZ-TRZ as a yellow solid. The yield was over 84%. This material was further purified by sublimation under reduced pressure for OLED fabrication. [NMR] ^1H NMR (CDCl_3 , 300 MHz) δ = 6.05 (d, 4H), 6.62 (t, 4H), 6.68 (t, 4H), 6.72 (d, 4H), 7.58 (m, 7H), 8.81 (d, 2H), 9.00 (d, 4H); ^{13}C NMR (CDCl_3 , 300 MHz) δ = 113.3, 115.7, 121.7, 123.3, 131.2, 131.8, 133.9, 143.4, 144.0, 171.3. [MS] MALDI-MS m/z Calcd for $\text{C}_{45}\text{H}_{29}\text{N}_5\text{O}_2$, 671; found, 671. [Element analysis] Calcd for $\text{C}_{45}\text{H}_{29}\text{N}_5\text{O}_2$: C, 80.46; H, 4.35; N, 10.43. Found: C, 80.17; H, 4.20; N, 10.37.

2,4,6-Tri(4-bromophenyl)-1,3,5-triazine. The amount of 3.57 g of 4-bromobenzonitrile (19.6 mmol) was added to 9.99 g of trifluoromethane sulfonic acid cooled at 0–5 °C by ice-bath and stirred for 30 min. The mixture was further stirred at room temperature overnight. Subsequently, 50 mL of water was added to the mixture, and the resulting mixture was neutralized with sodium

hydroxide. Then, 50 mL of mixed solvent of chloroform/acetone = 50/50 was added to the above mixture, the organic layer was separated, and the aqueous layer was extracted with the mixed solvent. The combined organic layers were washed with brine, dried over Mg_2SO_4 , and concentrated in vacuo. Then, 3.34 g of 2,4,6-tri(4-bromophenyl)-1,3,5-triazine was obtained as a white solid. The yield was over 94%. This material was used in the next step without further purification. [NMR] ^1H NMR (CDCl_3 , 300 MHz) δ = 7.70 (d, 6H), 8.60 (d, 6H); ^{13}C NMR (CDCl_3 , 300 MHz) δ = 120.0, 128.3, 128.7, 129.0, 130.9, 132.4, 135.2, 136.1. [MS] MALDI-MS m/z Calcd for $\text{C}_{21}\text{H}_{12}\text{Br}_3\text{N}_3$, 546; found, 546.

2,4,6-Tri(4-(10*H*-phenoxazin-10*H*-yl)phenyl)-1,3,5-triazine (tri-PXZ-TRZ). To a solution of 1.09 g of 2,4,6-tri(4-bromophenyl)-1,3,5-triazine (2.00 mmol), 1.22 g of phenoxazine (6.60 mmol), and 2.74 g of potassium carbonate (19.8 mmol) in 60 mL of toluene was added, with stirring, a solution of 45.0 mg of palladium (II) acetate (0.20 mmol) and 148 mg of tri-*tert*-butylphosphine (0.73 mmol) in 60 mL of toluene. Subsequently, the mixture was stirred and refluxed for one day. The cooled mixture was partitioned between chloroform and water. The organic layer was separated, and the aqueous layer was extracted with chloroform. The combined organic layers were washed with brine, dried over Mg_2SO_4 , and concentrated in vacuo. Column chromatography of the residue solid (eluent, chloroform/hexane = 1:1) afforded 1.65 g of tri-PXZ-TRZ. The yield is over 97%. This material was further purified by sublimation under reduced pressure for OLED fabrication. [NMR] ^1H NMR (CDCl_3 , 300 MHz) δ = 6.06 (d, 6H), 6.63 (t, 6H), 6.69 (t, 6H), 6.73 (d, 6H), 7.60 (d, 6H), 9.01 (d, 6H); ^{13}C NMR (CDCl_3 , 300 MHz) δ = 113.3, 115.6, 121.7, 123.3, 128.8, 129.1, 131.1, 131.7, 132.9, 133.9, 136.1, 143.2, 144.0, 171.1. [MS] MALDI-MS m/z Calcd for $\text{C}_{57}\text{H}_{36}\text{N}_6\text{O}_3$, 853; found, 853. [Element analysis] Calcd for $\text{C}_{57}\text{H}_{36}\text{N}_6\text{O}_3$: C, 80.27; H, 4.25; N, 9.85. Found: C, 80.34; H, 4.07; N, 9.82.

■ ASSOCIATED CONTENT

📄 Supporting Information

Synthetic routes and additional photophysical properties of bis-PXZ-TRZ and tri-PXZ-TRZ discussed in the text. CCDC 937721 for bis-PXZ-TRZ. This material is available free of charge via the Internet at <http://pubs.acs.org>.

■ AUTHOR INFORMATION

Corresponding Author

*(C.A.) E-mail: adachi@opera.kyushu-u.ac.jp.

Notes

The authors declare no competing financial interest.

■ ACKNOWLEDGMENTS

This research was supported by the Funding Program for World-Leading Innovative R&D on Science and Technology (FIRST Program) and the International Institute for Carbon Neutral Energy Research (WPI-I2CNER), sponsored by the Japanese Ministry of Education, Culture, Sports, Science and Technology. We acknowledge Ms. H. Nomura and Ms. N. Nakamura for performing TG-DTA measurements and sublimation and Mr. T. Matsumoto for X-ray crystal structure analysis. Computations were partly carried out using the computer facilities at the Research Institute for Information Technology, Kyushu University.

■ REFERENCES

- (1) Endo, A.; Ogasawara, M.; Takahashi, A.; Yokoyama, D.; Kato, Y.; Adachi, C. *Adv. Mater.* **2009**, *21*, 4802–4806.
- (2) Uoyama, H.; Goushi, K.; Shizu, K.; Nomura, H.; Adachi, C. *Nature* **2012**, *492*, 234–238.
- (3) Pohl, R.; Montes, V. A.; Shinar, J.; Anzenbacher, P., Jr. *J. Org. Chem.* **2004**, *69*, 1723–1725.

- (4) Zhao, Q.; Yu, M.; Shi, L.; Liu, S.; Li, C.; Shi, M.; Zhou, Z.; Huang, C.; Li, F. *Organometallics* **2010**, *29*, 1085–1091.
- (5) Zachariasse, K. A.; Druzhinin, S. I.; Bosch, W.; Machinek, R. *J. Am. Chem. Soc.* **2004**, *126*, 1705–1715.
- (6) (a) Endo, A.; Sato, K.; Yoshimura, K.; Kai, T.; Kawada, A.; Miyazaki, H.; Adachi, C. *Appl. Phys. Lett.* **2011**, *98*, 083302. (b) Lee, S. Y.; Yasuda, T.; Nomura, H.; Adachi, C. *Appl. Phys. Lett.* **2012**, *101*, 093306. (c) Zhang, Q.; Li, J.; Shizu, K.; Huang, S.; Hirata, S.; Miyazaki, H.; Adachi, C. *J. Am. Chem. Soc.* **2012**, *134*, 14706–14709.
- (7) (a) Nakagawa, T.; Ku, S.-Y.; Wong, K.-T.; Adachi, C. *Chem. Commun.* **2012**, *48*, 9580–9582. (b) Tanaka, H.; Shizu, K.; Miyazaki, H.; Adachi, C. *Chem. Commun.* **2012**, *48*, 11392–11394. (c) Mehes, G.; Nomura, H.; Zhang, Q.; Nakagawa, T.; Adachi, C. *Angew. Chem., Int. Ed.* **2012**, *51*, 11311–11315.
- (8) (a) Grabowski, A. W.; Rotkiewicz, K.; Rettig, W. *Chem. Rev.* **2003**, *103*, 3899–4031. (b) Bhattacharyya, K.; Chowdhury, M. *Chem. Rev.* **1993**, *93*, 507–535. (c) Rettig, W. *Angew. Chem., Int. Ed.* **1986**, *25*, 971–988.
- (9) Frisch, M. J.; et al. *Gaussian 09*, revision C. 01; Gaussian, Inc.: Wallingford, CT, 2009.
- (10) Chai, J.-D.; Head-Gordon, M. *J. Chem. Phys.* **2008**, *128*, 084106.
- (11) Dunning, J. T. H. *J. Chem. Phys.* **1989**, *90*, 1007–1023.
- (12) Martin, R. *J. Chem. Phys.* **2003**, *118*, 4775–4777.
- (13) Bauernschmitt, R.; Ahlrichs, R. *Chem. Phys. Lett.* **1996**, *256*, 454–464.
- (14) Casida, M. E.; Jamorski, C.; Casida, K. C.; Salahub, D. R. *J. Chem. Phys.* **1998**, *108*, 4439–4449.
- (15) Reichardt, C. *Chem. Rev.* **1994**, *94*, 2319–2358.
- (16) Jia, M.; Ma, X.; Yan, L.; Wang, H.; Guo, Q.; Wang, X.; Wang, Y.; Zhan, X.; Xia, A. *J. Phys. Chem. A* **2010**, *114*, 7345–7352.